THE ASTROPHYSICAL JOURNAL, 536:368–379, 2000 June 10

A TOY MODEL OF GIANT MOLECULAR CLOUDS

ANTHONY ALLEN AND FRANK H. SHU
Astronomy Department, University of California, Berkeley, Berkeley, CA 94720-3411
Received 1999 August 13; accepted 2000 January 26

ABSTRACT

We idealize giant molecular clouds as flattened sheets, incorporating the concepts of strong magnetization, star formation from dense cores, and efficient bipolar outflows. This toy model reproduces the observed tendency of molecular clouds to form filaments without the need to invoke large-scale overall gravitational collapse that would yield a rate of star formation far in excess of empirical Galactic values. It yields line width–size relationships that are in rough accord with observations, although better simulations are needed that remove the imposition of periodic boundary conditions and allow for a more systematic treatment of subgrid turbulence. The model lends credence to earlier ideas concerning the self-regulation of star formation by turbulence and photoionization.

Subject headings: ISM: clouds — ISM: jets and outflows — ISM: kinematics and dynamics — MHD — stars: formation

1. INTRODUCTION

Millimeter-wave radio maps of giant molecular clouds (GMCs) reveal that they frequently have a filamentary structure (e.g., Bally et al. 1987; Mizuno et al. 1995; Falgarone et al. 1998; Nakahama et al. 1998; Wiseman & Ho 1998). Motivated by similar phenomena in cosmology (see the review of Bertschinger 1998), some workers have performed numerical simulations to explain the formation of such filamentary clouds as the products of the gravitational collapse and fragmentation of nonmagnetized gaseous configurations containing many thermal Jeans masses (e.g., Klessen, Burkert, & Bate 1998; Nagai, Inutsuka, & Miyama 1998).

Gravitational collapse along the shortest available dimension (first into sheets, then into lines, then into points) is a viable option for cosmology because the free-fall timescale $t_{\rm ff}$ in that problem is automatically of the same order as the age of the universe (in models having approximately the closure density). The average density $\langle\rho\rangle$ in molecular clouds is 8 orders of magnitude times higher than the closure density of the universe; thus, the corresponding free-fall time $t_{\rm ff} \propto \langle\rho\rangle^{-1/2}$ is 4 orders of magnitude lower than the age of the universe. Large pieces of molecular clouds cannot be converting into stars on a free-fall timescale without exceeding by 2 orders of magnitude the known rate of star formation in the Galaxy, 3–5 $M_\odot$ yr^{-1} (Scalo 1986; Evans 1999). In particular, Zuckerman & Evans (1974) point out that the large line widths seen in most molecular clouds cannot have an origin in large-scale gravitational collapse, precisely because such an interpretation would lead to far too fast a turnover of molecular gas into stars.

Most astronomers today believe that large GMC line widths are associated with magnetohydrodynamic (MHD) waves and turbulence (Arons & Max 1975; Shu, Adams, & Lizano 1987; Myers & Goodman 1988; McKee et al. 1993). Numerical simulations of MHD turbulence in multiple spatial dimensions show that sheets and filaments develop naturally as a result of the dissipation of this turbulence (Mac Low et al. 1998; Padoan & Nordlund 1999; Ostriker, Gammie, & Stone 1999). The same simulations indicate the decay of free turbulence is rapid, only weakly dependent on the degree of magnetization of the cloud and occurring on a timescale comparable to an eddy crossing time. For self-gravitating, virialized, clouds the latter is comparable to the free-fall time, which revives the conundrum of too fast a rate of star formation, unless (1) there is an efficient replenishment of cloud turbulence (McKee 1989) or (2) the levels of magnetization in most GMCS make them close to marginally critical objects (Shu et al. 1999). In this paper, we shall combine the two possibilities.

Many researchers (e.g., Norman & Silk 1980; Lada 1985; Welch et al. 1985; Fukui et al. 1986; McKee 1989; Bally et al. 1999) have proposed that the mechanism responsible for the replenishment of GMC turbulence is bipolar outflows from young stellar objects (YSOs) (Cudworth & Herbig 1979; Snell, Loren, & Plambeck 1980; Rodriguez, Ho, & Moran 1980). A popular model supposes that YSOs have disks that transport mass inward at a rate $\dot{M}_D$ either by MHD instabilities (Balbus & Hawley 1992) or by spiral density-waves (e.g., Laughlin, Korchagin, & Adams 1998), but before reaching the star, a magnetocentrifugal mechanism turns a fraction f of $\dot{M}_D$ into a disk wind of mass-loss rate $\dot{M}_{\rm w}$ (e.g., Pudritz & Norman 1986; Shu et al. 1988):

$$\dot{M}_{\rm w} = f\dot{M}_D \,. \tag{1}$$

In the generalized X-wind model, $f \approx \frac{1}{3}$ (Shu et al. 1994, 2000).

A highly flattened configuration is locally subcritical or supercritical if the ratio of the mass per unit area Σ to the flux per unit area (the vertical component of the magnetic field) B_z, measured in units of $(2\pi G)^{-1/2}$, where G is the universal gravitational constant, has a value

$$\lambda \equiv (2\pi G)^{1/2}\,\frac{\Sigma}{B_z}\,, \tag{2}$$

which is, respectively, less than or greater than unity (Mestel & Spitzer 1956; Li & Shu 1996). Conversely, if we model turbulent support as a polytropic or logatropic scalar pressure with a relatively soft equation of state (e.g., Lizano & Shu 1989; Holliman & McKee 1993), then all sub-Alfvénic magnetostatic configurations with $\lambda \le 1$ are highly flattened in the z-direction normal to the sheet (e.g., Galli et al. 1999).

Consider an *isopedic* sheet with arbitrary variations of $\Sigma(x, y, t)$ but with spatially constant λ, which remains temporally constant because of field freezing. If this sheet is

isolated in space (i.e., vanishing magnetic and gravitational fields as $z \to \pm\infty$), the magnetic tension force exerted in the plane of the sheet ($z = 0$) is a negatively scaled version of self-gravity, with the constant of proportionality equal to $-1/\lambda^2$ (Shu & Li 1997). In other words, the repulsive tendency of magnetic forces exceeds the attractive tendency of self-gravity for subcritical clouds, $\lambda < 1$, and such objects have to be confined, at least in part, by external pressure. Highly subcritical configurations with $\lambda \ll 1$ are therefore diffuse clouds, not molecular clouds. Moreover, because the thermal Jeans mass is much less than the total mass of a GMC, and because any initial turbulence supporting the cloud is soon dissipated, highly supercritical GMCs with $\lambda \gg 1$ are likely to have disappeared from the Galaxy long ago by gravitational collapse. Thus, GMCs in the Galaxy today are probably everywhere close to being marginally critical, $\lambda \sim 1$ (say, within a factor of 2), which is a conclusion supported by empirical Zeeman measurements of many regions (e.g., Heiles et al. 1993; Crutcher 1999).

2. A TOY MODEL

In this section, we adopt as a toy model the hypothesis that molecular clouds are spatially flat sheets with an exactly critical level of magnetization, $\lambda = 1$. We further suppose that thermal pressure is negligible at scales $\gg 0.1$ pc of primary interest here. Below 0.1 pc, clouds need to be treated as fully three-dimensional objects since thermal pressure in cloud cores gains in importance relative to the other forces of the problem (Myers 1995; Goodman et al. 1998). Empirically, structure associated with turbulence appears to persist down to very small scales, although some debate exists concerning its exact form (cf. Elmegreen & Falgarone 1996; Blitz & Williams 1997; and Falgarone et al. 1998). In this work, except for a crude treatment of subgrid turbulence in § 5, we abandon any attempt to describe dynamics below the grid scale of 0.1 pc. On scales larger than 0.1 pc in flattened clouds, we may self-consistently ignore both the gas and magnetic pressures but not the magnetic tension (see Shu & Li 1997). With field freezing, magnetic forces then exactly balance gravitational forces for all times in the sheet. Because there are no net forces in the problem if we explicitly treat the above-grid turbulence as actual motions rather than as some sort of artificial eddy stress, the equations of motion are especially simple: Small pieces of the sheet move at constant speed in a straight line until they collide with other small pieces of the sheet. When different pieces of the sheet do collide, the shock jump conditions (for a zero-temperature sheet) are also simple: The collision occurs inelastically, with the conservation of total mass and vector momentum of the various pieces and with the removal of all relative motion along the line of centers after the pieces coagulate. Observations by Williams & Myers (1999) and Lee, Myers, & Tafalla (1999) of converging motions on scales appreciably larger than 0.1 pc toward starless cores may be symptomatic of this mechanism for forming dense structures in molecular clouds.

Continual dissipation of energy occurs when pieces of the sheet intersect and merge into filaments. The self-gravity in a dense filament would be intense, but it would be balanced by an opposite and equally intense magnetic tension created by all the field lines that bunch together tightly in the midplane while spreading out quickly above and below the sheet. We predict therefore that magnetic field lines thread mainly *perpendicularly* to the long axes of well-defined filaments, in a cylindrical fan above and below the sheet.

Exact force balance would be lost, however, if the condition of field freezing breaks down. Ambipolar diffusion and thermal pressure (relative to "turbulent pressure") become important effects when cloud surface and volume densities rise beyond certain threshold values (McKee 1989; Li, Evans, & Lada 1997). For the simulation that follows, we assume that ambipolar diffusion becomes very efficient when the local surface density Σ, averaged over a unit cell (representing a molecular cloud core of typical diameter 0.1 pc) in a grid-based scheme, rises to $R = 100$ times the global value $\Sigma_{\rm avg}$ averaged over the entire computational box. In § 4 we shall vary the threshold ratio $R \equiv \Sigma_{\rm max}/\Sigma_{\rm avg}$ by factors of 10 in both directions (by changing $\Sigma_{\rm avg}$) and examine the corresponding changes in the rate of star formation.

It is perhaps a new theoretical concept that on a global scale in GMCs, magnetic forces effectively cancel self-gravity (an exact consequence for a $\lambda = 1$ cold sheet) and that it is only in dense cores (large and small) that molecular clouds become truly self-gravitating and therefore capable of forming stars. This concept may underlie the observational notion that, except for dense cores, molecular clouds are mainly sterile to star formation (Evans 1999), as well as the remarkable similarity between the fractal structures and turbulent properties seen in diffuse clouds (where self-gravity is universally agreed upon to be relatively unimportant) and in molecular clouds (see, e.g., Elmegreen 1999), with self-similarity breaking down in the latter only at the small scales of dense cores (Blitz & Williams 1997).

Nakano (1979) and Lizano & Shu (1989) suppose, as in the present paper, that the dimensionless mass-to-flux ratio λ in the background cloud starts with a value close to unity. They find via three-dimensional axisymmetric calculations that λ needs to increase by ambipolar diffusion only by a factor of ~ 2 before quasi-static contraction of a cloud's core reaches a pivotal state of sufficient central concentration as to ensure its subsequent gravitational collapse (see also Li & Shu 1996, 1997). The timescale associated with bringing magnetically supportable regions at $\lambda = 1$, which are shielded from all forms of ionizing radiation other than Galactic cosmic rays (see § 5), to pivotal states at $\lambda = 2$, where thermal pressure is also a substantial part of the overall support against self-gravity, occupies perhaps a few times 10^5 yr. A similar timescale is associated with the inside-out gravitational collapse of such pivotal states to give star formation (Shu 1977; A. Allen & F. H. Shu 2000, in preparation). Both processes have a much shorter duration than the evolutionary time of tens of Myr that characterize the GMC simulations of this paper. On a timescale of tens of Myr, we may approximate the formation of individual stars to occur instantaneously.

The calculations of Ciolek & Mouschovias (1994) and Basu & Mouschovias (1994) for two-dimensional axisymmetric sheets seemingly come to a different conclusion, but their cloud envelopes have dimensionless mass-to-flux ratios $\lambda \sim 0.02$. Condensation by ambipolar diffusion from such highly subcritical configurations (whose surfaces need to be kept from expanding by artificial boundary conditions) require unrealistically long times to produce gravitationally unstable cores. In our model, tens of Myr are required for outflows and turbulence to shove matter tens of pc at typical speeds of 1 or 2 km s^{-1}, but once dense fragments have been assembled by such a turbulent velocity

field (Nakano 1998), their further condensation into cloud cores and collapse into stars (and disks) is very fast.

In all of the simulations presented in this paper, we start with 32 particles in each of 256 × 256 cells (i.e., a total of 2,097,152 gas particles), with the cell length in the x- and y-directions being 0.1 pc. Calculations with 8 times fewer particles yield grainier but similar results (see, e.g., Shu et al. 1999). We have also carried out simulations with 4 times more particles and noticed no important changes. For the case $R = 100$, when any cell acquires 3200 particles, 256 particles are assumed to form one or more stars; 128 particles [corresponding to $f/(1-f) = 128/256 = \frac{1}{2}$, i.e., to a fraction $f = \frac{1}{3}$] are ejected in the form of a bipolar wind with a terminal velocity v_w equal to 230 km s^{-1}. The corresponding momentum input, 29,440 particles km s^{-1}, is immediately shared by the 2944 ambient particles in the cell (128 in the original wind plus 2816 in the cell that did not participate in the gravitational collapse but got swept up in the outflow); thus, a molecular outflow of 10 km s^{-1} carried by these 2944 particles impinges on neighboring cells as a result of the star formation process in a dense core.

For definiteness we imagine the mass in an active cell (represented by 3200 particles when $R = 100$, by 320 particles when $R = 10$, etc.) equals the typical 11 $M_\odot$ core that Onishi et al. (1998) find per star-forming event in the Taurus molecular cloud. The corresponding visual extinction to the center of the precollapse core (halfway through it) is then 25 magnitudes. When $R = 100$, $\Sigma_{avg} = 32$ particles per cell then yields 0.5 visual mag of extinction in the perpendicular direction to background sources and double this value, or $A_V = 1$ mag, in a typical slant direction. This extinction characterizes the kind of cloud that we are simulating.

The assignments of the mass of each particle, the velocity of outflows, and the length scale of the computational grid are arbitrary, and the reader may prefer to use other numbers by appropriate rescalings. With our scaling, the total momentum imparted by a typical bipolar outflow over its entire life history is ~ 100 $M_\odot$ km s^{-1}, an order of magnitude larger than conventional values sometimes cited in the literature for observed molecular outflows from low-mass YSOs (see the reviews of Lada 1985 and Bachiller 1996). However, observations of parsec-long optical jets demonstrate that YSO outflows are episodic, with many sources having blown through their surrounding cloud cores; thus, outflows are much longer lived than earlier estimates based on apparent sizes and flow speeds (Reipurth, Bally, & Devine 1997). These developments support an optimistic estimate for the total momentum input from YSO outflows.

In Figure 1, contours of gravitational equipotential are calculated with periodic boundary conditions in the x-y directions and are plotted on a gray scale. Iso–surface density contours would look similar but with much greater contrast ratios, a failing of the models to which we shall return in § 5. The simulations are started with a uniform and smooth surface density distribution, except that the 32 particles in each cell are given random spatial positions. They are also given small x and y velocities (of order 2 km s^{-1}) that vary sinusoidally with spatial position on the above-grid scale.

For each YSO that forms, we assume that an outflow is ejected within wedges of effective opening angle 45° aligned parallel and antiparallel to the spin angular momentum vector of the inner edge of the YSO accretion disk. The asymptotic behavior of the X-wind has a more complex behavior (Shu et al. 1995), and the resulting outflow and blowout are also shaped by the spatial dependence of the surrounding molecular cloud core (Li & Shu 1996), but we have not attempted to account for such details in an idealized simulation in two dimensions. We further assume that magnetic braking of the precollapse cloud core tends to align the spin vector parallel to the local direction of the interstellar magnetic field $\boldsymbol{B}$ (see Mouschovias & Paleologou 1980 for relative efficiencies of braking for the parallel and perpendicular rotators). In such a model, YSO outflows align with $\boldsymbol{B}$ in the ambient medium. On the rationale that stars are unlikely to form exactly in the midplane of the sheet, and to keep the calculation (artificially) two-dimensional, we thus orient the bipolar outflow axes along the local direction of the horizontal component of the magnetic field just above or below the midplane of the sheet. This orientation rule yields the only reason to calculate the geometries of the gravitational and magnetic fields, since, in their dynamical influence on the gas not inside stars, they are assumed always to balance.

We follow the fate of the ejected wind by the same dynamic laws as the cloud gas. Thus, the bipolar outflows sweep up ambient gas into thin moving shells that obey vector momentum conservation. This process resupplies the "turbulence" that is lost elsewhere through inelastic collisional agglomeration. The individual moving shells also eventually merge to form new dense filaments and cores that give rise to further generations of young stars and outflows.

Figure 1*a* yields the configuration after 2.5 Myr of evolution, when the system still reflects the near-periodicity of the starting conditions. At 15 Myr, the configuration as displayed in Figure 1*b* has lost all memory of the initial conditions. Small dense cores have formed that have given birth to stars with outflows. The directions of the outflows can be deduced by noting that the magnetic field $\boldsymbol{B}$ is locally parallel (or antiparallel) to the gravitational field $\boldsymbol{g}$ everywhere, and the components of $\boldsymbol{g}$ (in the x- and y-directions) are, of course, perpendicular to the equipotential contours that are being plotted in Figure 1.

The eye easily picks out filaments in all of the three later figures. The filaments are dotted by dense cores along their length. Once there is any tendency for elongation in the x-y plane, the associated magnetic field orientations favor outflows that are directed along the short axis of that elongation. (For a vivid demonstration that nature might have reproduced this tendency, see Yu, Bally, & Devine 1997.) These bipolar outflows then sweep up ambient gas that also tends to form elongated structures with similar spatial orientations. Two adjacent parallel filaments firing outflows at each other reinforce the compressional tendency, although they also ultimately blast each other apart.

Figure 1*c* shows the situation after 27.5 Myr. Although cloud filaments and cloud fragments exist throughout the map, notice that the overall region is in neutral force balance. Gravitational collapse is not occurring anywhere except at the centers of the densest cloud cores. Figure 1*d* depicts the configuration after 47.5 Myr, when 45% of the original mass of the cloud has been turned into stars, which are distributed more or less uniformly throughout this region (although some have migrated out of the original computational area, to be replaced by stars from neighboring areas because of the periodic boundary conditions). The

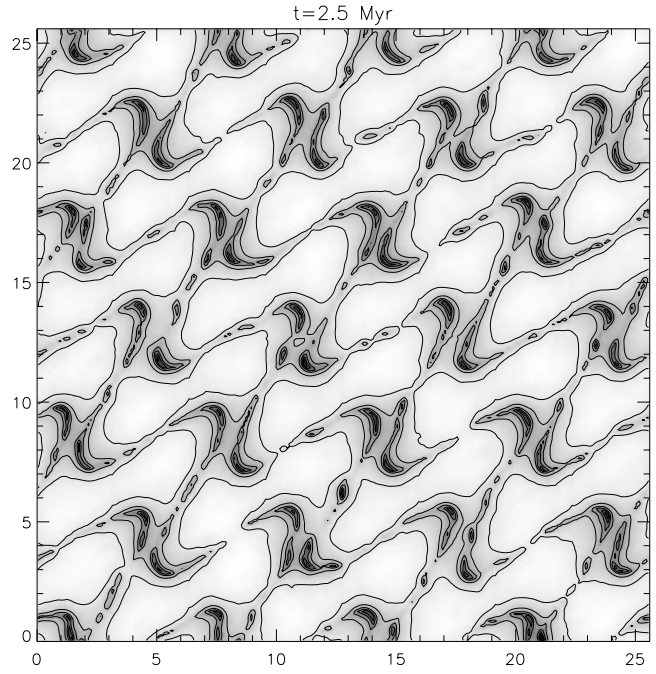

FIG. 1*a*

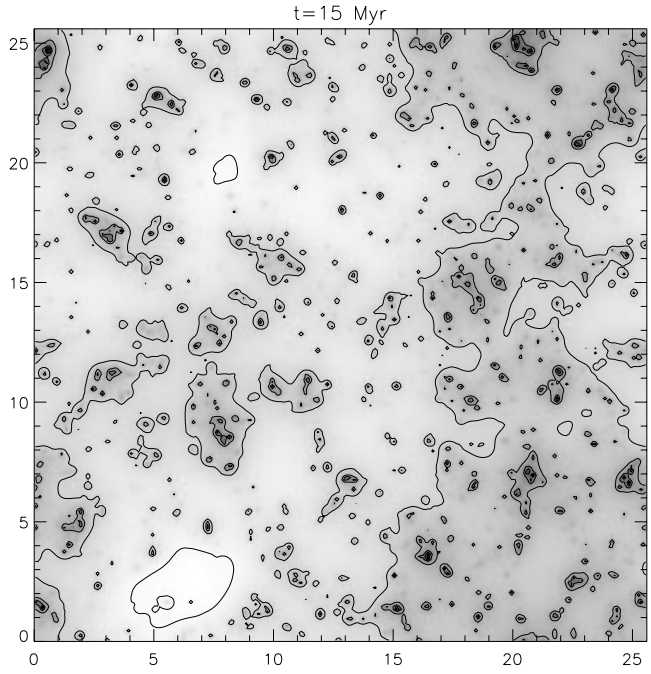

FIG. 1*b*

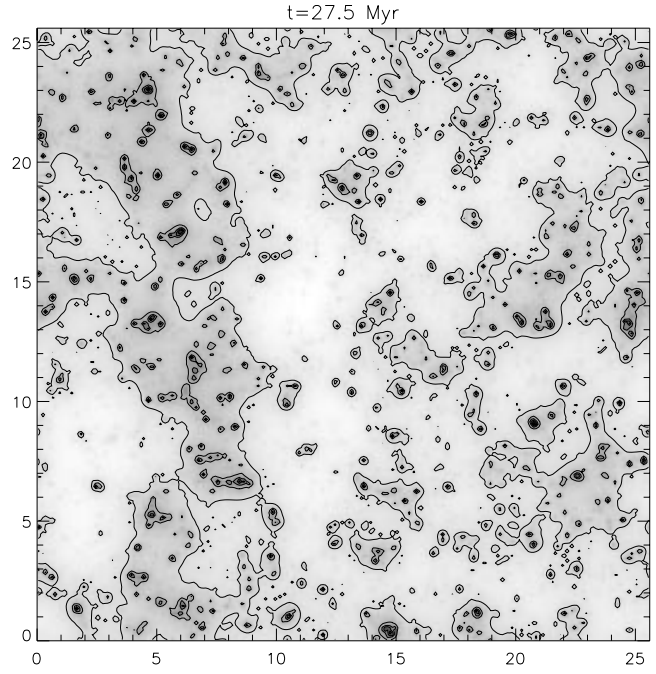

FIG. 1*c*

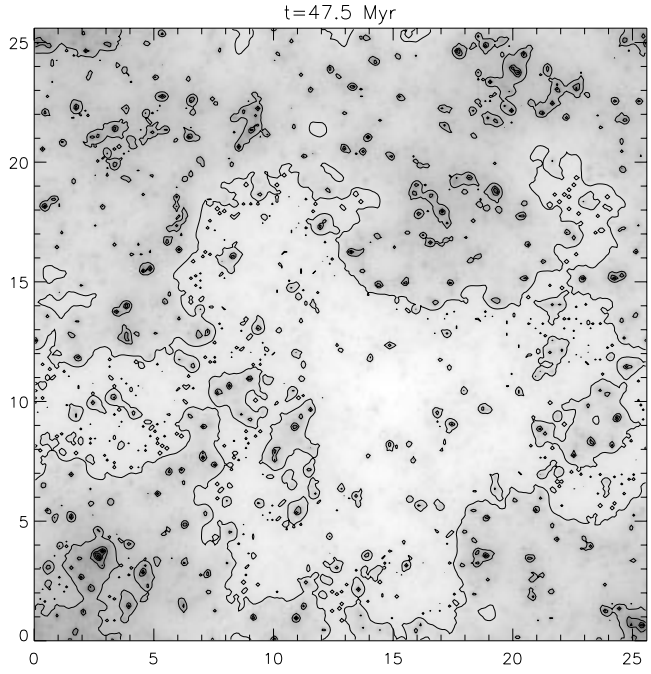

FIG. 1*d*

FIG. 1.—Equipotential plots of toy model simulation of the evolution of a $\lambda = 1$ molecular cloud sheet for the case $R = 100$ and no subgrid turbulence. Each side of the computational box measures 25.6 pc. (*a*): time of 2.5 Myr; (*b*): 15 Myr; (*c*): 27.5 Myr; (*d*): 47.5 Myr.

gas has been pushed by outflows in the interior toward the edges of the computational box, but the periodic boundary conditions prevent any permanent loss of gas from the region. This artificial feature probably makes our toy model longer lived than real GMCs. Moreover, the entire simulation has broken down by 47.5 Myr since a substantial fraction of the total initial mass has been converted into stars and is no longer threaded by the corresponding magnetic flux.

Our simulations resemble the independent work of Scalo & Chappell (1999), who also considered wind-driven models of star formation in a simplifying two-dimensional geometry, but in a finite-difference treatment of the fluid continuum rather than particles in a cell. Where they ignore self-gravity and magnetic fields, we explicitly invoke their balance in a critically magnetized cloud. Instead of bipolar outflows, Scalo & Chappell adopt isotropic winds, which are somewhat less effective in producing *long* filamentary

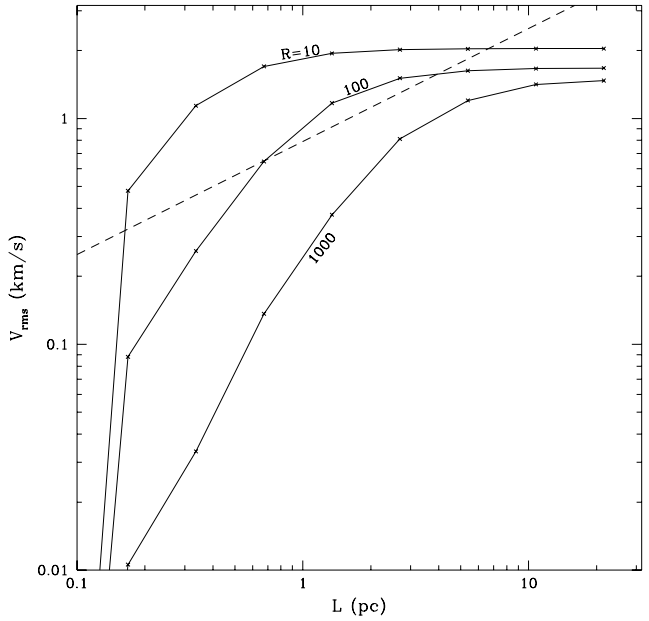

FIG. 2.—Line width–size relationship at 2.75, 27.5, and 275 Myr for the cases $R = 10$, 100, and 1000, when all three models have turned a similar fraction of gas into stars. The quantity v_{rms} is computed for a line of sight inclined at 45° with respect to the disk normal. All three simulations are performed with zero subgrid turbulence, so v_{rms} goes to zero by fiat below $L = 0.1$ pc.

structures than our calculations. It would be interesting to compute the two-point angular-correlation function for our models, as they do for theirs, but we believe such computation is premature until after the removal of periodic boundary conditions (see below).

3. LINE WIDTH–SIZE RELATIONSHIP

In the curve labeled $R = 100$ in Figure 2, we plot the line width–size relationship for the simulation in Figure 1 at a model time of 27.5 Myr. Corresponding plots at 15 and 47.5 Myr look very similar, except for minor differences attributable to either transients or the gradual depletion of cloud gas. The graphs in Figure 2 are computed from the rms velocity dispersion v_{rms} of gas particles measured along a line of sight inclined 45° with respect to the disk plane and over square regions of different sizes L. The dashed line represents Larson's (1981) law,

$$v_{rms} \propto L^{0.5} , \tag{3}$$

with the proportionality constant chosen so that $v_{rms} = 1$ km s^{-1} at $L = 1.6$ pc. The computed relationship departs from Larson's law (1) at small L because our rule for turbulent dissipation forces v_{rms} to go to zero inside any given cell for $L < 0.1$ pc and (2) at large L because our imposition of periodic boundary conditions forces sampling of identical regions once L exceeds 25.6 pc. Apart from the distortions produced by these two features (which may not be entirely ad hoc; see Myers & Gammie 1999), the computed line width–size relationship has roughly the right velocities at the corresponding length scales (cf. Myers 1995). In particular, it might have been thought (e.g., Fleck 1981) that any outflow model for cloud turbulence would produce the largest line widths at the smallest scales (from which the outflows emanate), which would be in contradiction with the positive exponent in Larson's law. This naive expectation overlooks the tendency, however, for YSO winds to drive large velocities in regions where the outflows channel into large relative voids, whereas they impart only small velocities when they sweep into small dense cores (see also Fleck 1983).

TABLE 1

CHARACTERISTIC TIMESCALE FOR STAR FORMATION τ_* WITH NO SUBGRID TURBULENCE

Percent in Stars	$R = 10$, $v_0 = 0$ (Myr)	$R = 100$, $v_0 = 0$ (Myr)	$R = 1000$, $v_0 = 0$ (Myr)
10	3.8	44	570
20	3.5	46	510
30	4.4	55	530
40	5.4	60	630

Also plotted in Figure 2 are the results from simulations in which every parameter is held the same as in Figure 1 except for the ratio $R \equiv \Sigma_{max}/\Sigma_{avg}$ of threshold and average surface densities. The star formation rates of the three cases, $R = 10$, $R = 100$, and $R = 1000$, are very different (see § 4), and the comparisons in Figure 2 have been made at simulation times when similar fractions of the GMC have been turned into stars. Figure 2 shows that the line width–size relationship does depend on the physical conditions of the underlying cloud, but the dependence is not a sensitive one. In particular, clouds of high average surface density (low R) have high rates of star formation and therefore high rates of turbulent energy injection, but they also have high rates of turbulent dissipation. The enhanced dissipation rate does not exactly offset the enhanced injection rate, yielding turbulent speeds that are somewhat larger in regions of more active star formation, but the effect is milder than one might have guessed when the mean star formation rate varies by 2 orders of magnitude (see Table 1). This result ameliorates a frequent criticism directed against the general approach: If YSO outflows stir GMC turbulence, why do we see similar levels of turbulence in clouds with very different levels of star formation?

4. STAR FORMATION RATE

Figure 3 displays the cumulative fraction of stars formed as a function of simulation time for the model of Figure 1. Notice that the cloud is completely sterile to star birth during the first 10 Myr. Because of transients introduced by the arbitrary initial conditions, simulation time is not a useful measure of cloud age or expected lifetime. Instead, we define a characteristic timescale for star formation, based on instantaneous quantities accessible to astronomical measurement:

$$\tau_* \equiv M_{GMC}/\dot{M}_* , \tag{4}$$

where $\dot{M}_*$ is the star formation rate of a cloud when the mass left in its gas is M_{GMC}. For the simulation of Figure 1, $\tau_* \approx 50$ Myr during its period of active star formation (see also Table 1). For the Galaxy as a whole, $M_{GMC} \approx 1 \times 10^9$ $M_\odot$ (Strong et al. 1988; Blitz 1993) and $\dot{M}_* \approx 4$ $M_\odot$ yr^{-1}, so the corresponding timescale $\tau_* \approx 250$ Myr.

Table 1 gives the resulting characteristic timescales τ_* for our simulations with different contrast ratios $R \equiv \Sigma_{max}/\Sigma_{avg}$ at simulation times when 10%, 20%, 30%, and 40% of the

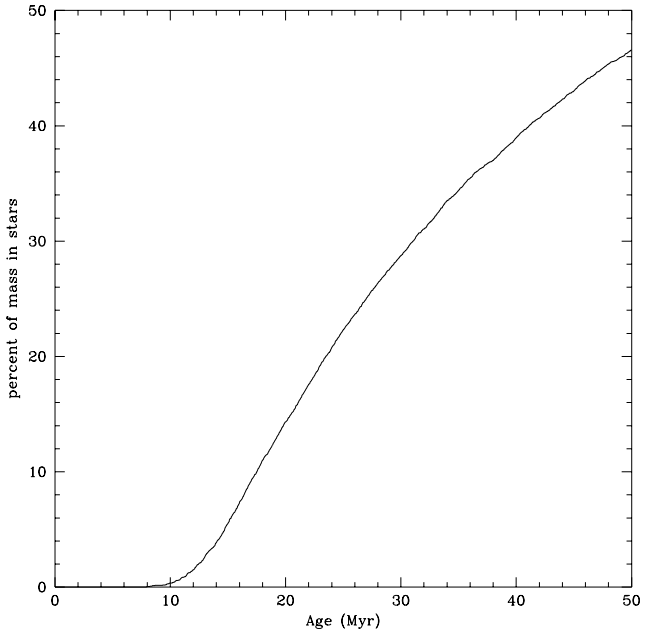

FIG. 3.—Mass accumulated in stars as a function of GMC evolutionary time for the case $R = 100$ and no subgrid turbulence.

original gas mass of the GMC has turned into stars. Notice that τ_* scales with $R \equiv \Sigma_{max}/\Sigma_{avg}$ approximately as $\tau_* \propto R$, which is what one expects for agglomeration theories of star formation from discrete cloudlets. In order for such models to yield a star formation timescale τ_* consistent with the current average in the Galaxy, $\tau_* \approx 250$ Myr, we would nominally require $R \approx 500$. Such a choice is too extreme a contrast ratio for most GMCs, and leads us to examine in § 5 the influence of subgrid turbulence.

5. SUBGRID TURBULENCE

The last two sections have revealed two principal inadequacies of the simulations presented so far: (1) they yield line width–size relationships that have too much curvature in a log-log plot, and (2) they yield too high a rate of star formation for realistic values of the contrast parameter $R \equiv \Sigma_{max}/\Sigma_{avg}$. There is a third failing that we have glossed over until now, and that is a tendency for the iso–surface density plots corresponding to the equipotential plots of Figure 1 to have too many regions of high and low density and too few regions of moderate density. All three discrepancies have a common cause.

In models in which gas particle encounters are taken to be perfectly inelastic, compressive flows that lead to collisions between parcels of gas can only add to, and never subtract from, the density of such parcels. Expansive flows that decrease Σ in the general turbulent field can and do occur in the simulations, but they are eliminated by fiat on the subgrid scale. Because all particles within a cell are constructed to have identical velocities, they move together in space as a unit, accumulating more mass as they sweep up loose parcels of gas. Thus, as the simulation proceeds, there is an irreversible buildup of parcels with large values of Σ, which eventually leads to too high a rate of star formation. The appearance of YSOs with bipolar outflows reverses the agglomeration process, but to rely on this mechanism as the only disruptive influence in the problem creates quasi-steady states that have the difficulties itemized in the previous paragraph.

It is, of course, a theoretical oversimplification to assume that the spectrum of turbulence induced by bipolar outflows, and followed explicitly by the simulations for scales above the size of the grid, suddenly stops at scales of the grid size and smaller. Moreover, empirical evidence exists that the spectrum of turbulent fluctuations continues to scales well below 0.1 pc (see, e.g., Falgarone et al. 1998). To include the effects of such turbulence, we adopt the following procedure. At each time step, after finding the average velocity in each cell, instead of giving every particle in the cell this same exact velocity, we add on x and y components randomly chosen for each particle to lie between 0 and $\pm v_0$, with v_0 equal to an eigenvalue (taken to be constant in time and space for a given value of R) of the self-consistent procedure described below. The correct choice for the case $R = 50$ turns out to be $v_0 = 0.195$ km s^{-1}, roughly what observations imply for scales of 0.1 pc (e.g., Myers 1995) and roughly what would be appropriate if we were to extrapolate by Larson's power law to the grid size of the calculation (see Fig. 6). We otherwise perform the simulations exactly as before.

The improvement in the simulation results is quite dramatic when the turbulent velocities on the subgrid scale have sufficient time to disperse incipient cloud cores before they accumulate even more mass by absorbing other parcels from the above-grid flows. Figure 4 shows the iso–surface density contours, plotted on a gray scale, for a simulation in which $R = 50$, with subgrid turbulence included as described in the previous paragraph. Figures 4*a* and 4*b*, at simulation times, respectively, of 5 and 20 Myr, clearly still retain memory of the sinusoidal starting conditions. Active star formation is well underway by the simulation times of 35 and 50 Myr of Figures 4*c* and 4*d*. In the latter two panels, short filaments a few pc long studded with dense cores show up more prominently than long filaments tens of pc long, although the eye, guided with sufficient imagination (or with the help of equipotential contours as in Fig. 1), can still trace out very elongated, partially broken, features. The main problem in comparing Figures 4*c* and 4*d* with observations is that real clouds do not exhibit nearly as many empty holes. This discrepancy undoubtedly arises because of the simplifying assumption that the GMC is a completely flat sheet and that outflows carve out cavities coplanar with this sheet. The situation is clearest in Figure 4*b*, where individual outflows can be seen that have swept-up parsec-scale biconical cavities in extended cloud gas left over from the initial conditions. One has the impression that the images would look more realistic if the outflow dynamics were not all projected into a single plane but were distributed in z also over scales of a pc or so (see the comments in Shu et al. 1987, p. 36). One also has the impression that Figures 4*c* and 4*d* are statistically too uniform to be maps of real giant molecular clouds. This blandness might be alleviated by simulations in which the momentum injection occurs by continuous outflows of finite duration and varying intrinsic power and is not input impulsively and all of the same strength as in the current calculations.

In Figure 5 we study the effects of taking an initial spatial periodicity in the perturbations that is twice that of Figure 4. The greater coherence in converging motions yields an earlier start to active star formation, and the lengths of the corresponding filaments are initially longer; however, the

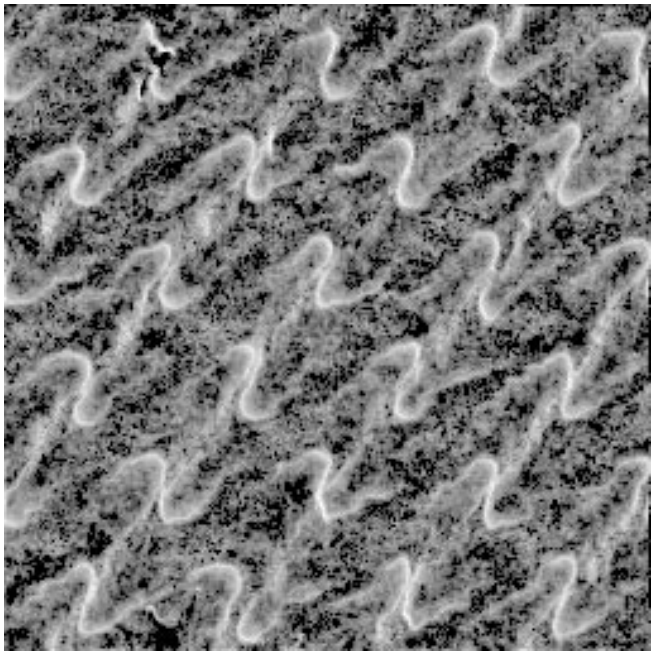

FIG. 4*a*

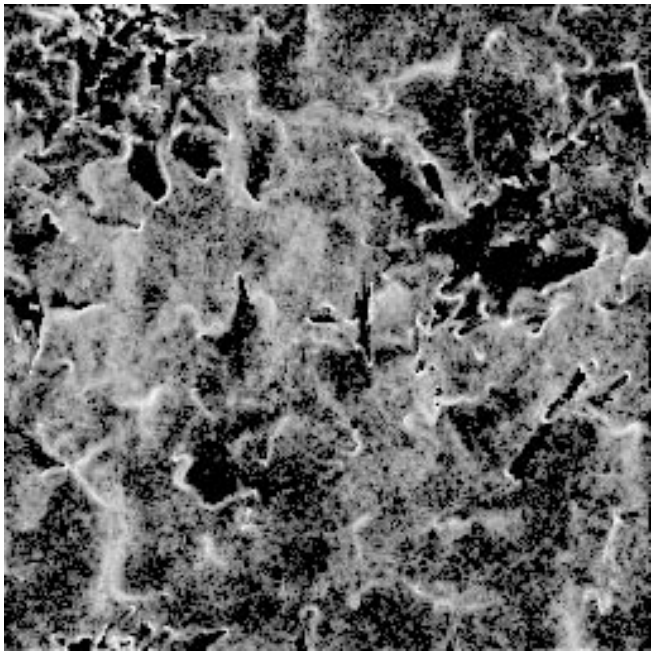

FIG. 4*b*

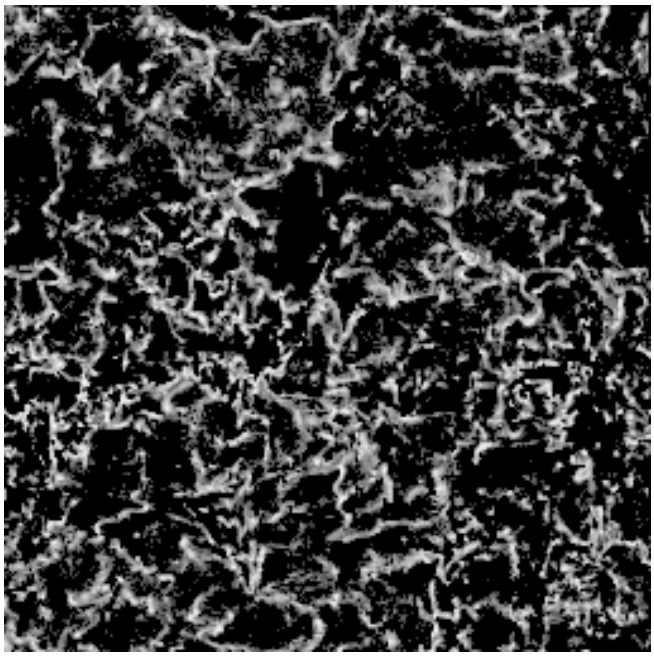

FIG. 4*c*

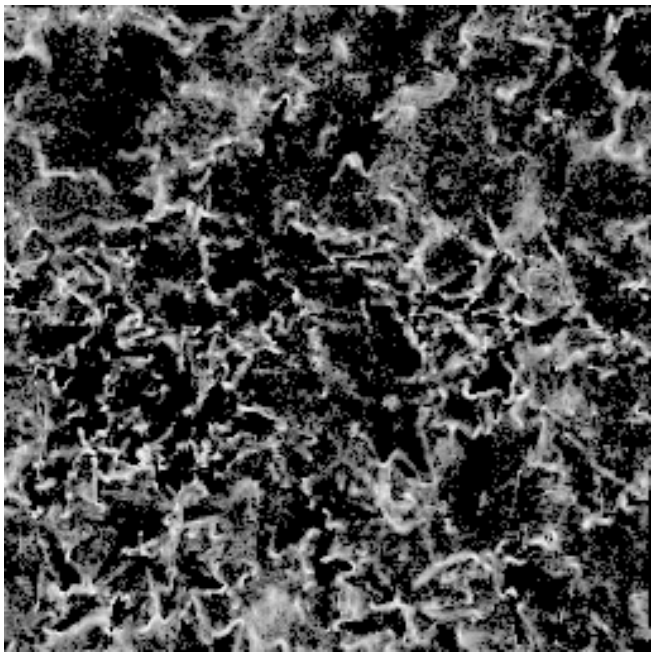

FIG. 4*d*

FIG. 4.—Gray-scale plots of iso–surface density for the case $R = 50$ and subgrid turbulence at a level $v_0 = 0.195$ km s^{-1}. Each side of the computational box measures 25.6 pc. (*a*): time of 5 Myr; (*b*): 20 Myr; (*c*): 35 Myr; (*d*): 50 Myr.

late-time behavior and appearance of Figures 4 and 5 are quite similar. Very long and well-aligned filaments in GMCs may require, therefore, special starting conditions—e.g., an origin via the Parker instability in spiral galactic shocks (Mouschovias, Shu, & Woodward 1974; Matsumoto & Shibata 1992); pursuit of this line of thought might yield insight into the formation mechanisms of GMCs in present-day spiral galaxies.

The curve labeled $v_0 = 0.195$ km s^{-1} in Figure 6 shows the corresponding line width–size relationship for the simulation of Figure 4 at a time at which 22% of the original GMC mass has turned into stars. (The corresponding diagram for the simulation of Fig. 5 looks very similar.) Notice that we now have a smooth transition at $L = 0.1$ pc from subgrid to above-grid scales. (The subgrid value is calculated before projection from $v_{\rm rms} = v_0/\sqrt{3}$ at a size $L = 0.05$ pc. Projection at a viewing angle of 45° to the sheet reduces line widths by a further factor $1/\sqrt{2}$.) The correct eigenvalue 0.195 km s^{-1} for v_0 is found by performing trial simulations with different values for v_0 until we achieve physical continuity and reasonableness in the line width–size relationship, i.e., *by the self-consistent*

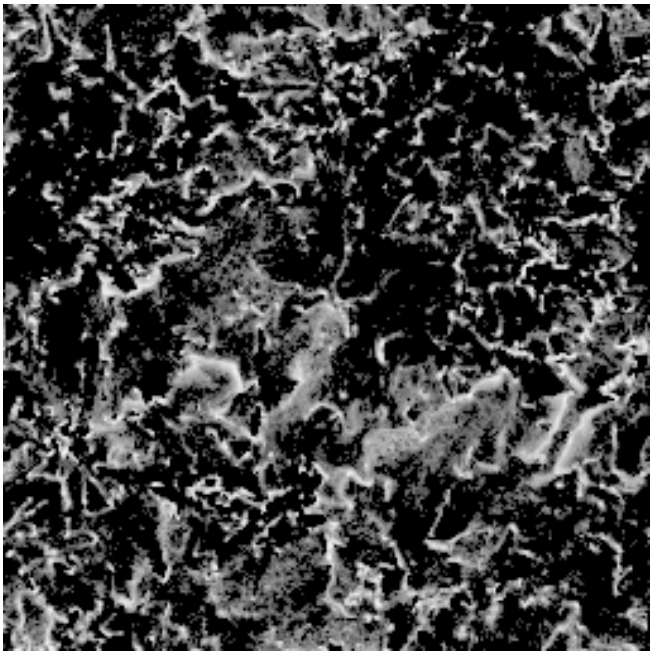

FIG. 5*a*

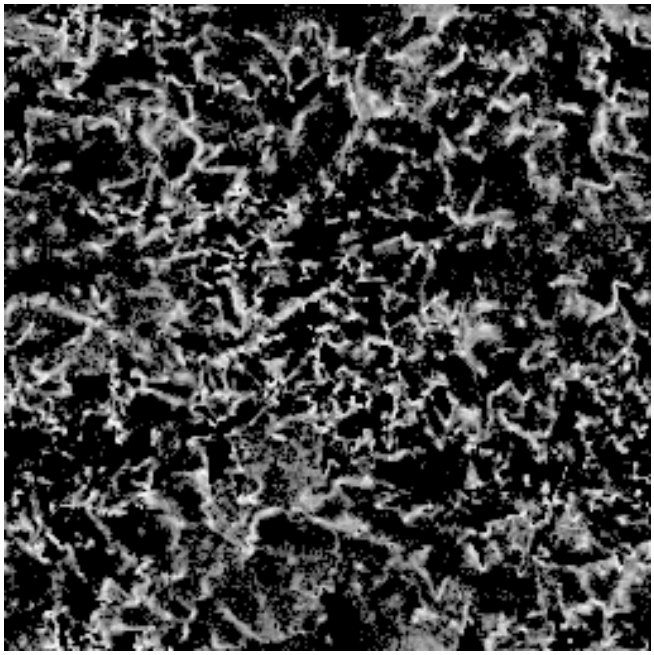

FIG. 5*b*

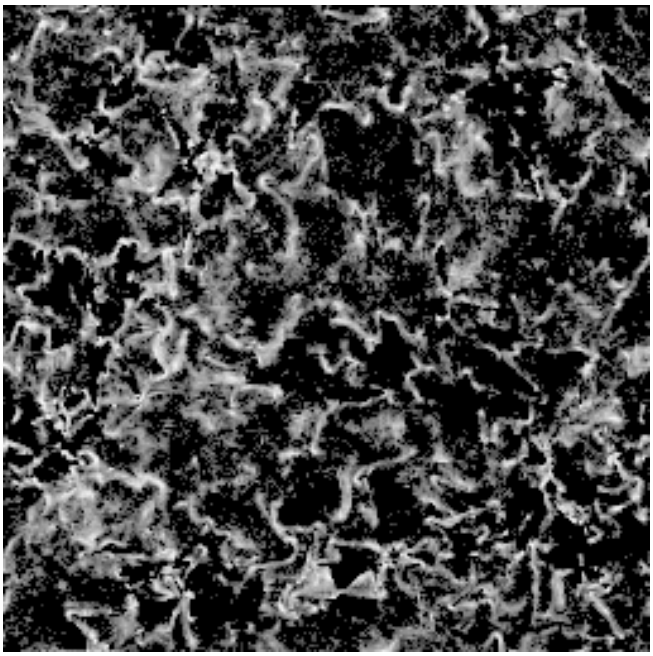

FIG. 5*c*

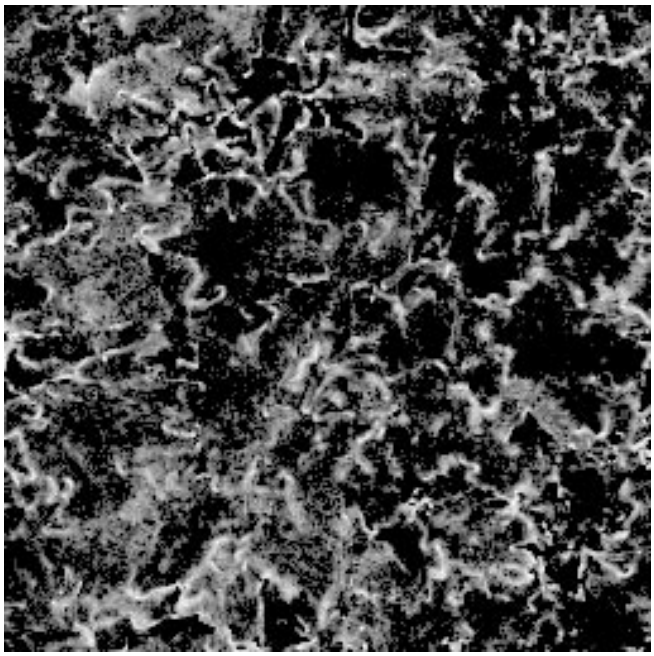

FIG. 5*d*

FIG. 5.—Gray-scale plots of iso–surface density for the case $R = 50$ and subgrid turbulence at a level $v_0 = 0.195$ km s^{-1}, but with a spatial period of the initial perturbations equal to twice that of Fig. 4. Each side of the computational box measures 25.6 pc. (*a*): time of 5 Myr; (*b*): 20 Myr; (*c*): 35 Myr; and (*d*): 50 Myr.

requirement that the subgrid-turbulence is sustainable by whatever mechanism maintains the turbulence at above-grid scales.

For illustrative purposes, Figure 6 also shows the resultant line width–size relationship when v_0 differs from the self-consistent eigenvalue $v_{sc} = 0.195$ km s^{-1}. When $v_0 = 0.150$ km s$^{-1} < v_{sc}$, cores assemble too readily, and star formation proceeds at too quick a pace, with a consequent injection of too much turbulence at larger than grid scales. One expects a raising of v_0 to occur, leading to a lowering of the core-accumulation and star formation rates. When $v_0 = 0.200$ km s$^{-1} > v_{sc}$, cores disperse too readily, and star formation proceeds at too slow a pace, with a consequent maintenance of turbulence at all scales little more than what is assumed (artificially) for subgrid values. One expects a lowering of v_0 to occur, leading to a raising of the core-accumulation and star formation rates. As Figure 6 indicates, the cessation of star formation with increasing subgrid turbulence occurs sharply for given contrast ratio R, almost as a phase transition. Thus, the determination of

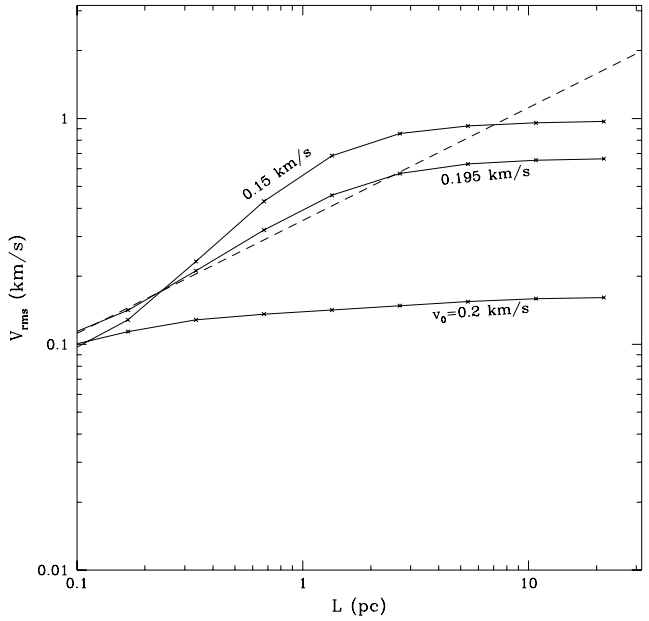

FIG. 6.—Line width–size relationship at 50 Myr for the case $R = 50$ at a time when 22% of the original GMC mass has turned into stars and when we assume three different levels of subgrid turbulence: $v_0 = 0.150$, 0.195, and 0.200 km s^{-1}. The quantity v_{rms} is computed for a line of sight inclined at 45° with respect to the sheet normal.

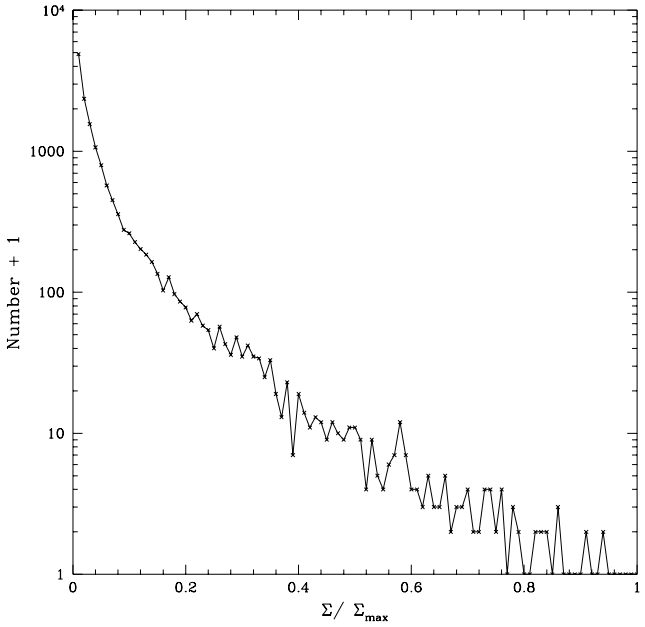

FIG. 7.—Histogram of number of cells (plus 1) vs. the normalized surface density Σ/Σ_{max} in those cells for the case of Fig. 4*d*.

v_{sc} is better bounded above than below. Conversely, for given subgrid turbulence v_0, the onset of star formation will occur sharply with decreasing contrast ratio R (increasing Σ_{avg}). Coupled with the similar findings of Lizano & Shu (1989) concerning the ability of too much turbulence to shut off dense core formation by ambipolar diffusion (in *subumbral* clouds), these results help to justify earlier speculations that turbulence (in addition to photoionization) may help to self-regulate the star formation rate in GMCs (e.g., Norman & Silk 1980; McKee 1989).

Figure 7 shows a histogram of the number of cells N containing surface density Σ in equally spaced bins for the self-consistent model of Figure 4. The abscissa of the graph is the normalized surface density Σ/Σ_{max}, and the ordinate is $N + 1$, where the 1 is added so that null bins can be sensibly plotted on a logarithmic scale. Most cells are occupied by relatively low density gas, accounting, perhaps, for the ease with which ultraviolet photons seemingly penetrate GMCs (e.g., Schneider et al. 1998). A very small percentage of the cloud mass is instantaneously in cores with Σ close to Σ_{max}, consistent with our assumption that the time spent in such dense states is very short.

Figure 8 shows the star formation history of the $R = 50$ model with the self-consistent level of subgrid turbulence determined, globally and for all time, as $v_0 = 0.195$ km s^{-1}. The corresponding characteristic star formation time τ_* is quite reasonable, 70–200 Myr, over the duration when star formation has consumed between 5% and 20% of the original GMC gas.

Table 2 summarizes some results for τ_* when we vary R and choose v_0 by the eigenvalue procedure described above. Notice that regions that are more dense on average (smaller R) have higher self-consistent levels of subgrid turbulence. The dissipation of the turbulent energy may also make such regions physically hotter than the conventional 10 K that arises by cosmic-ray heating. Such regions are known empirically to give birth to the formation of higher mass stars, which in turn yield more powerful outflows (see, e.g., Shu et al. 1987; Myers 1995; Plume et al. 1997; Evans 1999). None of these effects are incorporated into the present simulations. In the future, it would be desirable to develop time-dependent procedures for obtaining v_0 locally that properly account for the three-dimensional structure of cloud cores at subgrid scales, including some evaluation of the effects for the production of different stellar masses. Independent of this more ambitious overall program, we are encouraged that the inclusion of realistic values for subgrid turbulence reduces the need to appeal to high

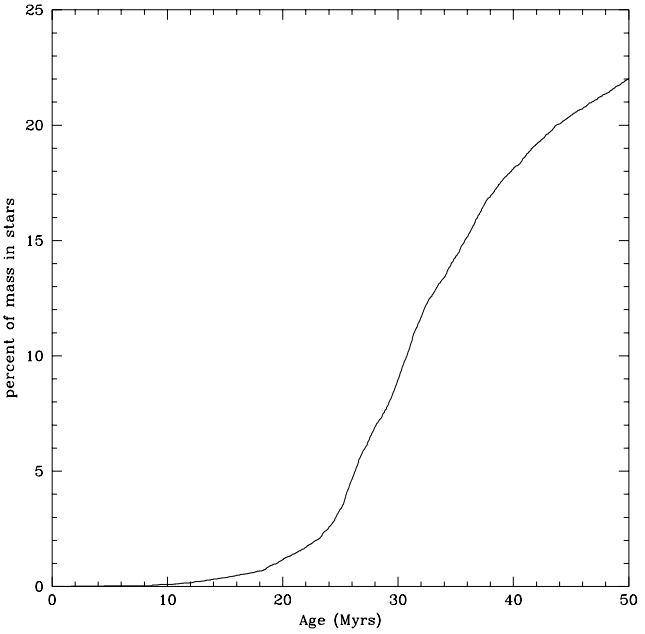

FIG. 8.—Mass accumulated in stars as a function of GMC evolutionary time for the case $R = 50$ and subgrid turbulence at a globally constant level $v_0 = 0.195$ km s^{-1}.

TABLE 2

CHARACTERISTIC TIMESCALE FOR STAR FORMATION τ_* WITH SUBGRID TURBULENCE v_0 AS LABELED

Percent in Stars	$R = 25$, $v_0 = 0.375$ km s^{-1} (Myr)	$R = 50$, $v_0 = 0.195$ km s^{-1} (Myr)	$R = 100$, $v_0 = 0.110$ km s^{-1} (Myr)
5	60	70	150
10	30	70	160
15	40	100	190
20	70	200	310

values of R to obtain model star formation rates in agreement with those from observations.

6. PHYSICAL INTERPRETATION AND SPECULATION

According to Table 2, models with R between 50 and 100 and with a level of turbulence on scales above and below the grid size consistent with driving by outflows from low-mass YSOs yield inverse star formation rates that are typical of the average GMC in the Galaxy, $\tau_* \sim 250$ Myr. What is the physical significance of a contrast ratio, say, $R \equiv \Sigma_{max}/\Sigma_{avg} \sim 50$? If Σ_{max} is a physical constant $\sim 10^3\ M_\odot$ pc^{-2} in different regions of active star formation, then $R \sim 50$ implies $\Sigma_{avg} \sim 20\ M_\odot$ pc^{-2}, which corresponds to a visual extinction of ~ 1 mag perpendicularly through the molecular sheet, or ~ 2 mag at a typical slant path through it. The last number is not unreasonable for a GMC (see, e.g., Blitz 1993), especially if we consider that our averaging procedure over the entire computational volume includes significant numbers of wind-blown cavities.

The value for $\Sigma_{max} \sim 10^3\ M_\odot$ pc^{-2} is also interesting. The corresponding visual extinction to such a core center is 25 mag, which is somewhat too large to attribute to the cutoff of ionizing far-ultraviolet photons (cf. McKee 1989). It is closer to the column density for the exclusion of soft X-rays, and it may be that X-rays from neighboring YSOs (e.g., Silk & Norman 1983; Glassgold, Feigelson, & Montmerle 2000) play an additional role to ultraviolet radiation in preventing much ambipolar diffusion from occurring, until cores form with A_V to their centers that exceed 25 mag and that can shield out all ionizing radiation except for Galactic cosmic rays (Lepp 1994; Helmich et al. 1995). The calculations are a little too crude at this point in the development of the theory to place too much credence on a specific value for the threshold visual extinction; we would merely claim that observations and theory are currently both consistent with the idea that photoionization of some sort provides a regulating influence on star formation additional to that provided by turbulence.

As noted before, Tables 1 and 2 are consistent with the rough scaling $\tau_* \propto R$ when the GMC has reached a quasi–steady state. Thus, the characteristic time for star formation τ_* can become comparable to the free-fall time of $\sim$a few Myr, only in those rare entire regions where R approaches unity and Σ_{avg} approaches Σ_{max}, i.e., where entire large regions consist of material at essentially core densities. This finding appears roughly consistent with the studies of clustered star formation by Lada et al. (1991) and Hillenbrand (1997).

What explains the wide variety of values of R encountered in different molecular cloud regions? The methods of this paper, which postulate given values of the background surface density Σ_{avg} in critically magnetized calculations with periodic boundary conditions, cannot provide an answer to this question. We need to consider unconstrained GMC models in which λ exceeds unity, moderately, even on a large scale. The greatest modification to result from such studies will be the tendency toward virialization that is necessitated by the presence of unbalanced gravitational and magnetic forces (cf. Matzner & McKee 1999). This process will cause a GMC—or pieces of it, such as large dense cores, where cluster star formation occurs (e.g., Lada 1999)—of a given mass M to expand or contract to a size L that is virially consistent with the level of turbulence and magnetically diluted gravitational forces that are present in the local simulation. The combination M/L^2 will then define a typical background surface density that would replace the Σ_{avg} used in the present simulations. It is to be hoped that self-consistent investigations of this type (that include the effects of YSO feedback) will give a first principles understanding of the differences between clustered and distributed star formation (see Evans 1999).

7. DISCUSSION

The toy model introduced in this paper clearly has its limitations when we attempt to apply it to the real world. Removing some of these limitations (e.g., the periodic boundary conditions) would not represent hard work; removing others (e.g., the two-dimensionality of the calculations) would require abandoning simplifying basic properties of the toy model (e.g., the Shu & Li 1997 theorems) and would add considerable computational effort. An important physical addition for future efforts would be to incorporate the effects of ambipolar diffusion and flux redistribution (and perhaps UV and X-ray photoionization) on the subgrid scale by separate computation, using the outer-scale two-dimensional results as boundary conditions for an inner-scale three-dimensional calculation. The resulting departures from isopedic conditions (i.e., variable λ) would introduce some complications, but it would still be possible to handle the gravitational and magnetic forces on the large scale as two scalar-potential fields.

Another interesting topic to explore in future models is the role of high-mass star formation, which may be especially relevant in regions of high average surface density (low values of R; e.g., Heaton et al. 1985; Kurtz et al. 2000). High-mass stars have much more powerful winds than low-mass stars (Churchwell 1999), and their H II regions help to photoevaporate incipient molecular cloud cores (Arthur & Lizano 1997) as well as the nebular disks (proplyds) around T Tauri stars (O'Dell, Wen, & Hu 1993; Johnstone, Hollenbach, & Bally 1998). Indeed, a complete model of GMC structure and evolution should not only compute the feedback effects of high-mass stars on the cloud but should also

explain what are the conditions required in the cloud to obtain the formation of these objects in the first place.

After the above improvements are implemented, it might be worthwhile to use clump-finding algorithms in the model maps to measure the number of clumps $\mathcal{N}(M)dM$ between mass M and $M + dM$ for comparison with the canonical observational result $\mathcal{N}(M) \propto M^{-1.5}$ (e.g., Williams, de Geus, & Blitz 1994). Unless there are departures from $\lambda = 1$, "clumps" exist only as turbulent fluctuations and not as entities, since gravitational and magnetic forces are everywhere in neutral balance above the grid scale. In $\lambda = 1$ models, it is similarly meaningless to discuss issues such as the connection between density-size and line width–size relationships within the context of the virialization of molecular clouds (cf. Myers & Goodman 1988).

Despite its weaknesses, our toy model may contain some elements of essential truth. In particular, we see many advantages to the hypothesis that GMCs (or large clumps within them), unlike their cores, are highly flattened structures, rather than fully three-dimensional objects. Fully three-dimensional clouds that are extended in the mean direction of the magnetic field and that are marginally critical necessarily have small subunits that are highly subcritical (since the mass scales with the cube of size but the flux scales only as the square). A value of $\lambda \ll 1$ makes the formation of self-gravitating cloud cores extremely slow and difficult. As Mestel (1965) was the first to point out, flattened clouds do not suffer this disadvantage, although the fragmentation of such objects may occur in a somewhat different way than originally envisaged by him. In particular, in the presence of a turbulent velocity field, flattened clouds that are only marginally critical ($\lambda \sim 1$) rather than highly supercritical ($\lambda \gg 1$) can form fragments without undergoing global gravitational collapse. (Gravitational fragmentation, in contrast to turbulent fragmentation, is difficult even for $\lambda = 1$ sheets; see Shu & Li 1997.)

But how do we reconcile the theoretical desirability of having flattened clouds with the observational difficulty discussed in § 5 that bipolar outflows of parsec scale do not look as if they are propagating into highly flattened structures? The answer may lie in the expected half-thickness for the local layer,

$$z_0 \approx \left(\frac{a^2 + \langle v_t^2 \rangle}{\pi G \langle \Sigma \rangle}\right)\left(\frac{\langle \lambda^2 \rangle}{\langle \lambda^2 \rangle + \langle \eta^2 \rangle}\right), \qquad (5)$$

where a is the isothermal sound speed, v_t is the z-component of the turbulent velocity, and η is the ratio of the horizontal gravitational field and $2\pi G\Sigma$ (see eqs. [1.3] and [2.28] of Shu & Li 1997). In equation (5), we have heuristically added turbulent support in quadrature to a^2, and angle brackets refer to averages over horizontal length scales comparable to $2z_0$. For simplicity, let us ignore the factor $\langle \lambda^2 \rangle / (\langle \lambda^2 \rangle + \langle \eta^2 \rangle)$ associated with magnetic pinch. For $\langle \Sigma \rangle = 20\ M_\odot\ \mathrm{pc}^{-2}$, then, equation (5) implies $z_0 > 1$ pc, where $\langle v_t^2 \rangle^{1/2}$ exceeds 0.6 km s^{-1}. For $\langle \Sigma \rangle = 80\ M_\odot\ \mathrm{pc}^{-2}$, it implies z_0 is less than half our nominal grid length of 0.1 pc when $\langle v_t^2 \rangle$ drops below the typical local sound speed $a \sim 0.2$ km s^{-1}. We might expect the first situation to apply in extended regions where outflows propagate once they break through their local molecular cloud cores. We might expect the second to apply in UV-shielded regions in which fragments arising from the dissipation of a turbulent velocity field undergo further condensation by ambipolar diffusion and form true molecular cloud cores. These cores with $\lambda \approx 2$, relatively free of turbulence, and supported against self-gravity as much by thermal pressure as by magnetic fields, are the sites for future star formation.

In such a picture, star-forming cloud cores are "islands of calm in a turbulent sea" (Goodman et al. 1998). Converging turbulent flows are a precursor to core production and a promoter of star formation (Nakano 1998; Williams & Myers 1999; Myers & Lazarian 1999), while diverging turbulent flows are a precursor to cloud destruction and a regulator of too rapid a rate of star formation (Norman & Silk 1980; Matzner & McKee 1999). Variations along these themes may yield a promising scheme for understanding the ubiquitous presence of filamentary chains of dense cores in GMCs that does not require global gravitational collapse with its attendant untenably high rates of star formation.

This research is supported by the National Science Foundation and by the NASA Astrophysical Theory Program which funds a joint Center for Star Formation Studies at NASA/Ames Research Center, the University of California at Berkeley, and the University of California at Santa Cruz. We thank Leo Blitz, Al Glassgold, Charlie Lada, Susana Lizano, Chris McKee, Phil Myers, Eve Ostriker, and Jean-Francois Panis for enlightening discussions.

REFERENCES

Arons, J., & Max, C. E. 1975, ApJ, 196, L77
Arthur, S. J., & Lizano, S. 1997, ApJ, 484, 810
Bachiller, R. 1996, ARA&A, 34, 111
Balbus, S. A., & Hawley, J. F. 1992, ApJ, 400, 610
Bally, J., Reipurth, B., Lada, C. J., & Billawala, Y. 1999, AJ, 117, 410
Bally, J., Stark, A. A., Wilson, R. W., & Langer, W. D. 1987, ApJ, 312, L45
Basu, S., & Mouschovias, T. Ch. 1994, ApJ, 432, 720
Bertschinger, E. 1998, ARA&A, 36, 599
Blitz, L. 1993, in Protostars & Planets III, ed. E. H. Levy & J. I. Lunine (Tucson: Univ. Arizona Press), 125
Blitz, L., & Williams, J. P. 1997, ApJ, 488, L145
Churchwell, E. 1999, in The Origin of Stars and Planetary Systems, ed. C. J. Lada & N. D. Kylafis (Dordrecht: Kluwer), 515
Ciolek, G. E., & Mouschovias, T. C. 1994, ApJ, 425, 142
Crutcher, R. M. 1999, ApJ, 520, 706
Cudworth, K. M., & Herbig, G. H. 1979, AJ, 84, 548
Elmegreen, B. G. 1999, in The Physics and Chemistry of the Interstellar Medium, ed. V. Ossenkopf, J. Stutzki, & G. Winnewisser (Berlin: GCA-Verlag Herdecke), 77
Elmegreen, B. G., & Falgarone, E. 1996, ApJ, 471, 816
Evans, N. J. 1999, ARA&A, 37, 311
Falgarone, E., Panis, J.-F., Heithausen, A., Pérault, M., Stutski, J., Puget, J.-F., & Bensch, F. 1998, A&A, 331, 669
Fleck, R. C. 1981, ApJ, 246, L151
———. 1983, ApJ, 272, L45
Fukui, Y., Sugitani, K., Takaba, H., Iwata, T., Mizuno, A., Ogawa, H., & Kawabata, K. 1986, ApJ, 311, L85
Galli, D., Lizano, S., Li, Z. Y., Adams, F. C., & Shu, F. H. 1999, ApJ, 521, 630
Glassgold, A. E., Feigelson, E. D., & Montmerle, T. 2000, in Protostars and Planets IV, ed. V. Mannings, A. P. Boss, & S. S. Russell (Tucson: Univ. Arizona Press), in press
Goodman, A. A., Barranco, J. A., Wilner, D. J., & Heyer, M. H. 1998, ApJ, 504, 223
Heaton, B. D., Matthew, N., Little, L. T., & Dent, W. R. F. 1985, MNRAS, 217, 485
Heiles, C., Goodman, A. A., McKee, C. F., & Zweibel, E. G. 1993, in Protostars & Planets III, ed. E. H. Levy & J. I. Lunine (Tucson: Univ Arizona Press), 279
Helmich, F. P., et al. 1995, in Physics and Chemistry of Interstellar Molecular Clouds, Proc. 2nd Cologne-Zermatt Symp., ed. G. Winnewisser & G. C. Pelz (Berlin: Springer), 254
Hillenbrand, L. 1997, AJ, 114, 198

Holliman, J. H., & McKee, C. F. 1993, BAAS, 182, 611
Johnstone, D., Hollenbach, D., & Bally, J. 1998, ApJ, 499, 758
Klessen, R. S., Burkert, A., & Bate, M. R. 1998, ApJ, 501, L205
Kurtz, S., Cesaroni, R., Churchwell, E., Hofner, P., & Walmsley, C. M. 2000, in Protostars & Planets IV, ed. V. Mannings, A. P. Boss, & S. S. Russell (Tucson: Univ Arizona Press), in press
Lada, C. J. 1985, ARA&A, 23, 267
Lada, E. A. 1999, in The Origin of Stars and Planetary Systems, ed. C. J. Lada & N. D. Kylafis (Dordrecht: Kluwer), 441
Lada, E. A., Evans, N. J., Depoy, D. L., & Gatley, I. 1991, ApJ, 371, 171
Larson, R. B. 1981, MNRAS, 194, 809
Laughlin, G., Korchagin, V., & Adams, F. C. 1998, ApJ, 504, 905
Lee, C. W., Myers, P. C., & Tafalla, M. 1999, ApJ, 526, 788
Lepp, S. 1994, in Astrochemistry of Cosmic Phenomenon, ed. P. Singh (Dordrecht: Reidel), 471
Li, W., Evans, N. D., & Lada, E. A. 1997, ApJ, 488, 277
Li, Z. Y., & Shu, F. H. 1996, ApJ, 472, 211
———. 1997, ApJ, 475, 237
Lizano, S., & Shu, F. H. 1989, ApJ, 342, 834
Mac Low, M. M., Klessen, R. S., Burkert, A., Smith, M. D., & Kessel, O. 1998, Phys. Rev. Lett., 80, 2754
Matsumoto, R., & Shibata, K. 1992, PASJ, 44, 167
Matzner, C., & McKee, C. F. 1999, in Star Formation 1999, ed. T. Nakamoto (Nagano: Nobeyama Radio Observatory), 353
McKee, C. F. 1989, ApJ, 345, 782
McKee, C. F., Zweibel, E. G., Goodman, A. A., & Heiles, C. 1993, in Protostars and Planets III, ed. E. H. Levy & J. I. Lunine (Tucson: Univ. Arizona Press), 327
Mestel, L. 1965, QJRAS, 6, 161
Mestel, L., & Spitzer, L. 1956, MNRAS, 116, 505
Mizuno, A., Onishi, T., Yonekura, Y., Nagahama, T., Ogawa, H., & Fukui, Y. 1995, ApJ, 445, L161
Mouschovias, T. Ch., & Paleologou, E. V. 1980, ApJ, 237, 877
Mouschovias, T. Ch., Shu, F. H., & Woodward, P. R. 1974, A&A, 33, 73
Myers, P. C. 1995, in Molecular Clouds and Star Formation, ed. C. Yuan & J. H. You (Singapore: World Scientific), 47
Myers, P. C., & Gammie, C. F. 1999, ApJ, 522, L141
Myers, P. C., & Goodman, A. A. 1988, ApJ, 329, 392
Myers, P. C., & Lazarian, A. 1998, ApJ, 507, L157
Nagai, T., Inutsuka, S., & Miyama, S. 1998, ApJ, 506, 306
Nakahama, T., Mizuno, A., Ogawa, H., & Fukui, Y. 1998, AJ, 1165, 336
Nakano, T. 1979, PASJ, 31, 697
———. 1998, ApJ, 494, 587
Norman, C., & Silk, J. 1980, ApJ, 238, 158
O'Dell, C. R., Wen, Z., & Hu, X. 1993, ApJ, 410, 696
Onishi, T., Mizuno, A., Kawamura, A., Ogawa, H., & Fukui, Y. 1998, ApJ, 502, 296
Ostriker, E. C., Gammie, C. F., & Stone, J. M. 1999, ApJ, 513, 259
Padoan, P., & Nordlund, A. 1999, ApJ, 526, 279
Plume, R., Jaffe, D. T., Evans, N. J., Martin-Pintado, J., & Gomez-Gonzalez, J. 1997, ApJ, 476, 730
Pudritz, R. E., & Norman, C. A. 1986, ApJ, 301, 571
Reipurth, B., Bally, J., & Devine, D. 1997, AJ, 114, 2708
Rodriguez, L. F., Ho, P. T. P., & Moran, J. M. 1980, ApJ, 240, L149
Scalo, J. 1986, Fundam. Cosmic Phys., 11, 1
Scalo, J., & Chappell, D. 1999, ApJ, 510, 258
Schneider, N., Stutzski, J., Winnewisser, G., Poglitsch, A., & Madden, S. 1998, A&A, 338, 262
Shu, F. H. 1977, ApJ, 214, 488
Shu, F. H., Adams, F. C., & Lizano, S. 1987, ARA&A, 25, 23
Shu, F. H., Allen, A., Shang, H., Ostriker, E. C., & Li, Z.-Y. 1999, in The Origin of Stars and Planetary Systems, ed. C. J. Lada & N. D. Kylafis (Dordrecht: Kluwer), 193
Shu, F. H., & Li, Z. Y. 1997, ApJ, 475, 251
Shu, F. H., Lizano, S., Ruden, S., & Najita, J. 1988, ApJ, 328, L19
Shu, F. H., Najita, J., Ostriker, E. C., & Shang, H. 1995, ApJ, 455, L155
Shu, F., Najita, J., Ostriker, E., Wilkin, F., Ruden, S., & Lizano, S. 1994, ApJ, 429, 781
Shu, F. H., Najita, J. R., Shang, H., & Li, Z.-Y. 2000, in Protostars and Planets IV, ed. V. Mannings, A. P. Boss, & S. S. Russell (Tucson: Univ. Arizona Press), in press
Silk, J., & Norman, C. 1983, ApJ, 272, L49
Snell, R. L., Loren, R. B., & Plambeck, R. L. 1980, ApJ, 239, L17
Strong, A. W., et al. 1988, A&A, 207, 1
Welch, W. J., Vogel, S. N., Plambeck, R. L., Wright, M. C. H., & Bieging, J. H. 1985, Science, 228, 1329
Williams, J. P., de Geus, E. J., & Blitz, L. 1994, ApJ, 428, 693
Williams, J. P., & Myers, P. C. 1999, ApJ, 518, L37
Wiseman, J., & Ho, P. T. P. 1998, ApJ, 502, 676
Yu, K. C., Bally, J., & Devine, D. 1997, ApJ, 485, L45
Zuckerman, B., & Evans, N. J. 1974, ApJ, 192, L149

Note added in proof (2000 April 18).—In a recent preprint, J. Chappel & D. Scalo (preprint [2000]) extend their two-dimensional simulations of wind-driven gas networks to include the effects of threshold star formation if cloud filaments pass a critical surface density for gravitational instability. Except for the lack of emphasis on magnetic fields, these ideas and calculations are similar to those reported in the present paper.